

# Raman scattering study of $\text{NaFe}_{0.53}\text{Cu}_{0.47}\text{As}$

W.-L. Zhang,<sup>1,\*</sup> Y. Song,<sup>2</sup> W.-Y. Wang,<sup>2</sup> C.-D. Cao,<sup>2,†</sup> P.-C. Dai,<sup>2</sup> C.-Q. Jin,<sup>3,4</sup> and G. Blumberg<sup>1,5,‡</sup>

<sup>1</sup>Department of Physics & Astronomy, Rutgers University, Piscataway, New Jersey 08854, USA

<sup>2</sup>Department of Physics and Astronomy and Rice Center for Quantum Materials, Rice University, Houston, Texas 77005, USA

<sup>3</sup>Beijing National Laboratory for Condensed Matter Physics and Institute of Physics, Chinese Academy of Sciences, Beijing 100190, China

<sup>4</sup>Collaborative Innovation Center of Quantum Matter, Beijing, China

<sup>5</sup>National Institute of Chemical Physics and Biophysics, Akadeemia tee 23, 12618 Tallinn, Estonia  
(Dated: November 12, 2021)

We use polarization-resolved Raman scattering to study lattice dynamics in  $\text{NaFe}_{0.53}\text{Cu}_{0.47}\text{As}$  single crystals. We identify four  $A_{1g}$  phonon modes, at 126, 172, 183, and 197  $\text{cm}^{-1}$ , and four  $B_{3g}$  phonon modes at 101, 139, 173, and 226  $\text{cm}^{-1}$  ( $D_{4h}$  point group). The phonon spectra are consistent with the  $Ibam$  space group, which confirms that the Cu and Fe atoms form a stripe order. The temperature dependence of the phonon spectra suggests weak electron-phonon and magneto-elastic interactions.

## I. INTRODUCTION

The parent compound of the iron-pnictide superconductor,  $\text{NaFeAs}$ , is a “bad metal.” It exhibits a tetragonal-to-orthorhombic transition at 52 K, a paramagnetic-to-spin-density wave transition at 41 K, and a superconducting transition at 23 K<sup>1</sup>. Doping copper into  $\text{NaFeAs}$  suppresses both the orthorhombic and the paramagnetic-to-spin-density-wave orders and enhances the superconductivity<sup>2-4</sup>. Recently, it was shown that heavy Cu substitution at the Fe site induces Mott-insulator-like behavior<sup>5,6</sup>. The electronic properties of the heavily doped  $\text{NaFe}_{1-x}\text{Cu}_x\text{As}$  are similar to those of lightly doped cuprates<sup>5,7,8</sup>.

For Cu substitution concentration  $x > 0.44$  a long-range collinear antiferromagnetic order with magnetic moments residing only at the Fe sites develops below 200 K. The moment increases with Cu concentration substitution  $x$ <sup>6</sup>. At the solubility limit near  $x = 0.5$ , new superlattice peaks appear in the TEM diffraction pattern, which are interpreted as the signature of Cu and Fe stripe order formation<sup>6</sup>, as depicted in the inset in Fig. 1. Compared to the parent  $\text{NaFeAs}$  compound in the tetragonal phase, the stripe-ordering of Cu and Fe in heavily doped  $\text{NaFe}_{1-x}\text{Cu}_x\text{As}$  removes the lattice four-fold rotational symmetry and reduces the crystallographic space group from  $Fmmm$  (point group  $D_{4h}$ ) to  $Ibam$  (point group  $D_{2h}$ ), making a structural analog of the magnetic order in parent  $\text{NaFeAs}$  crystals.

Here we present a polarization-resolved Raman scattering study of the lattice dynamics for  $\text{NaFe}_{0.53}\text{Cu}_{0.47}\text{As}$  single crystals. Four  $A_g$  phonon modes, at 126, 172, 183, and 197  $\text{cm}^{-1}$  and four  $B_{3g}$  phonon modes, at 101, 139, 173, and 226  $\text{cm}^{-1}$ , are identified. The phonon spectra are consistent with the Fe/Cu stripe-ordered structure. All the observed phonons exhibit a symmetric line shape. Across the antiferromagnetic phase transition, no phonon anomaly is observed. The data suggest weak electron-phonon and magneto-elastic interaction.

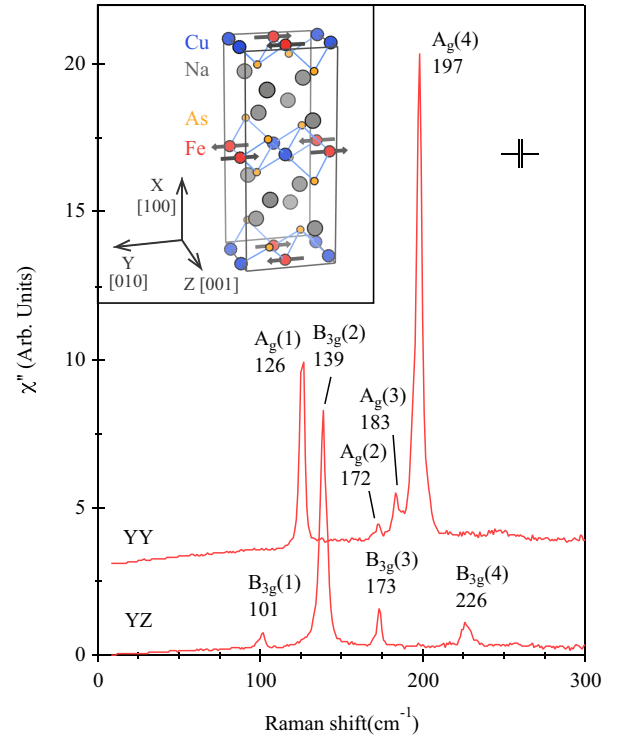


FIG. 1. Raman scattering spectra of  $\text{NaFe}_{0.53}\text{Cu}_{0.47}\text{As}$  crystals for  $YY + ZZ$  and  $YZ + ZY$  scattering geometries at 250 K measured with 1.9 eV excitation. The spectral resolution is 2.5  $\text{cm}^{-1}$ . Inset:  $\text{NaFe}_{0.5}\text{Cu}_{0.5}\text{As}$  unit cell with Cu and Fe collinear stripe order. Arrows at the Fe sites mark magnetic moments.

## II. EXPERIMENTAL

$\text{NaFe}_{1-x}\text{Cu}_x\text{As}$  single crystals were grown by the self-flux method<sup>6,9</sup>. The nominal Cu concentration was  $x = 0.85$ , which resulted in an actual concentration  $x = 0.47$ <sup>6</sup>. The preparation of the reference  $\text{LiFeAs}$  single crystal is described in<sup>10</sup>.

The  $\text{NaFe}_{1-x}\text{Cu}_x\text{As}$  crystal belongs to the  $Ibam$  space

TABLE I. Phonon mode decomposition at the  $\Gamma$  point and selection rules for Raman-active modes in  $Ibam$  space group.

		Irreducible representation
Acoustic		$B_{1u}+B_{2u}+B_{3u}$
IR		$3B_{1u}+5B_{2u}+5B_{3u}$
Raman		$4A_g+6B_{1g}+4B_{2g}+4B_{3g}$
Silent		$2A_u$
Atom	Wyckoff position	Raman active mode
Na	8j	$2A_g+2B_{1g}+B_{2g}+B_{3g}$
Fe	4b	$B_{1g}+B_{2g}+B_{3g}$
Cu	4a	$B_{1g}+B_{2g}+B_{3g}$
As	8j	$2A_g+2B_{1g}+B_{2g}+B_{3g}$

group at room temperature, as shown in the inset in Fig. 1. The crystallographic principal axis [001] of the  $Ibam$  group is along the Fe(Cu) stripe direction. We define the X, Y, and Z axes along crystallographic [100], [010], and [001] axes and Y'/Z' along the [011]/[0 $\bar{1}$ 1] direction (inset Fig. 2(a)).

There are 12 atoms in the primitive unit cell. Group theoretical analysis infers  $4A_g + 6B_{1g} + 4B_{2g} + 4B_{3g} + 2A_u + 4B_{1u} + 6B_{2u} + 6B_{3u}$ <sup>11</sup> symmetry decomposition of the 36 phonon modes at the Brillouin center  $\Gamma$  point. All the even  $g$  modes are Raman active. The irreducible representations and decomposition of the Raman active modes by symmetry are summarized in Table I.

Polarization-resolved low-temperature Raman scattering measurements were performed in a quasi-back scattering setup from natural cleaved (100) surface<sup>12</sup>. Polarizers with an extinction ratio better than 1:500 were employed<sup>13</sup>. Samples were cleaved in a nitrogen-filled glove bag and immediately transferred to an optical cryostat with continuous helium gas flow. We used 1.9 and 2.6 eV excitations from a Kr<sup>+</sup> laser, where the laser was focused on a  $50 \times 50 \mu m^2$  spot on the sample. The power was kept below 10 mW to minimize the laser heating. The local laser heating was estimated<sup>14,15</sup> and kept at less than 5 K. All referred temperatures are corrected for the laser heating.

The Raman scattering signal was analyzed with a triple-stage spectrometer with the spectral resolution setting at about  $2 \text{ cm}^{-1}$ . We used scattering geometries  $\mu\nu$  with  $\mu/\nu = Y, Z, Y'$  and  $Z'$ , where  $\mu\nu$  is short for  $\bar{X}(\mu\nu)X$  in Porto's notation. All spectra were corrected for the spectral response to obtain the Raman scattering intensity  $I_{\mu\nu}(\omega, T)$ . The Raman susceptibility  $\chi''_{\mu\nu}(\omega, T)$  was related to  $I_{\mu\nu}(\omega, T)$  by  $I_{\mu\nu}(\omega, T) = \chi''_{\mu\nu}(\omega, T)[1 + n(\omega, T)]$ , where  $n(\omega, T)$  is the Bose factor.

In Table II we list the Raman tensor for the  $D_{2h}$  group and the selection rule for experimentally accessible polarizations<sup>16</sup>. Due to the twin structure<sup>6</sup>, the collected signal from the (100) surface is a superposition of Raman scattering intensities from two types of orthogonal domains. For example, the signal for parallel polarized scattering geometry along the crystallographic axes con-

tains the intensity from YY geometry for one type of domain and ZZ geometry for the other type of domain. We denote this scattering geometry as YY + ZZ. Similarly, cross polarized signal along the crystallographic axes contains contributions from YZ and ZY geometries and is denoted YZ + ZY, and cross polarized signal along the diagonal directions contains contributions from Y'Z' and Z'Y' scattering geometries, is denoted Y'Z' + Z'Y'.

Following the notation in Table II, we assign all phonons that appear in the YY + ZZ geometry to the  $A_g$  symmetry modes, and those appear in the YZ + ZY geometry to the  $B_{3g}$  modes.

### III. RESULTS AND DISCUSSION

In Fig. 1 we show the Raman response for NaFe<sub>0.53</sub>Cu<sub>0.47</sub>As crystals at 250 K for YY + ZZ and YZ + ZY scattering geometries. We identify all the  $A_g$  and  $B_{3g}$  phonon modes predicted by group theory: four  $A_g$  symmetry modes, at 126, 172, 183, and 197  $\text{cm}^{-1}$ , and four  $B_{3g}$  symmetry modes, at 101, 139, 173, and 226  $\text{cm}^{-1}$ . All modes show a symmetric line shape.

We note that at the same frequency as the  $A_g$  phonon modes, some modes with a weaker intensity are also observed for the Y'Z' + Z'Y' geometry for both 2.6 and 1.9 eV laser excitations [Figs. 2(a)-(c)]. The intensity of the *leaking* modes is about 10% of the  $A_g$  phonon intensity in the YY+ZZ geometry, which is much higher than the experimental polarization extinction ratio. In Fig. 2(d) we show data for the LiFeAs tetragonal structure<sup>17</sup> measured employing the same setup. If the substituted Cu ions at Fe sites were randomly disordered,

TABLE II. Raman tensor and selection rules for Raman-active modes in the  $D_{2h}$  group.

		$R_{A_g} = \begin{bmatrix} a & 0 & 0 \\ 0 & b & 0 \\ 0 & 0 & c \end{bmatrix}$	$R_{B_{1g}} = \begin{bmatrix} 0 & d & 0 \\ e & 0 & 0 \\ 0 & 0 & 0 \end{bmatrix}$
		$R_{B_{2g}} = \begin{bmatrix} 0 & 0 & f \\ 0 & 0 & 0 \\ g & 0 & 0 \end{bmatrix}$	$R_{B_{3g}} = \begin{bmatrix} 0 & 0 & 0 \\ 0 & 0 & h \\ 0 & i & 0 \end{bmatrix}$
(001) surface	XX	YY	XY/YX
$A_g$	$a^2$	$b^2$	0
$B_{1g}$	0	0	$d^2/e^2$
(010) surface	XX	ZZ	XZ/ZX
$A_g$	$a^2$	$c^2$	0
$B_{2g}$	0	0	$f^2/g^2$
(100) surface	YY/ZZ	YZ/ZY	Y'Y'/Z'Z'    Y'Z'/Z'Y'
$A_g$	$b^2/c^2$	0	$(b+c)^2/4$ $(b-c)^2/4$
$B_{3g}$	0	$h^2/i^2$	$(h+i)^2/4$ $(h-i)^2/4$

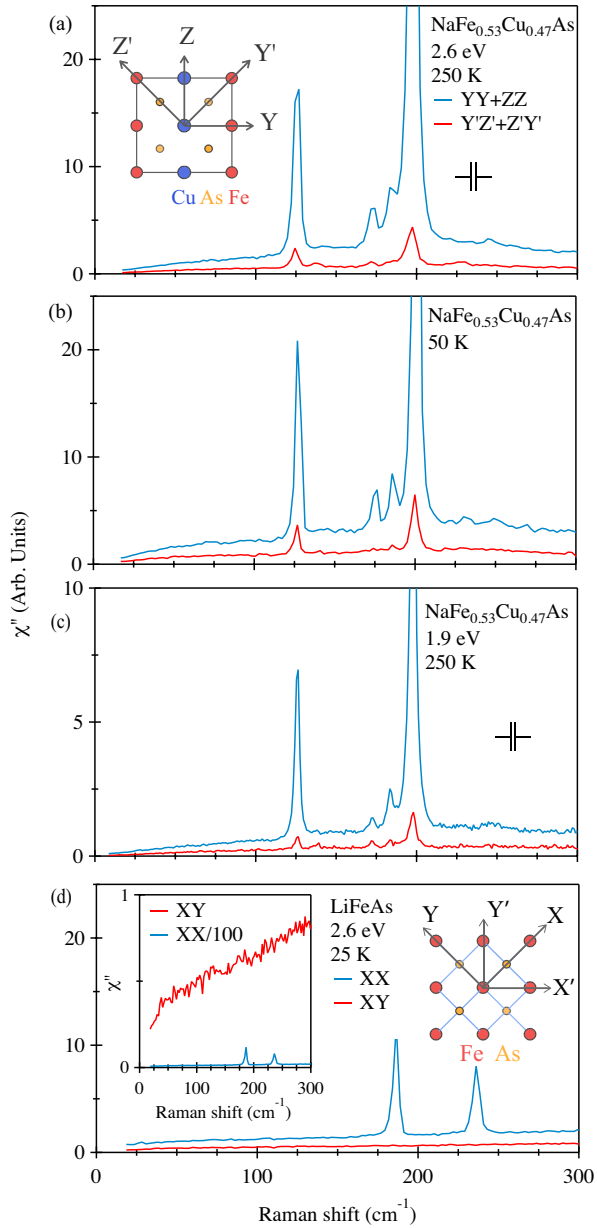


FIG. 2. (a, b)  $A_g$ -symmetry Raman active phonon modes measured for  $\text{NaFe}_{0.53}\text{Cu}_{0.47}\text{As}$  crystals at (a) 250 K and (b) 50 K in  $YY + ZZ$  (blue line) and  $Y'Z' + Z'Y'$  (red line) scattering geometries with 2.6 eV laser excitation with spectral resolution  $3.5 \text{ cm}^{-1}$ . Inset in (a): top view of the Fe-Cu-As layer for  $\text{NaFe}_{0.53}\text{Cu}_{0.47}\text{As}$  structure and the  $YZ-Y'Z'$  coordinates. (c) Same  $A_g$  phonon modes measured at 250 K with 1.9 eV excitation. (d) Raman spectra from tetragonal  $\text{LiFeAs}$  crystal at 25 K measured in  $X'X'$  (blue) and  $XY$  (red) scattering geometries with 2.6 eV-laser excitation. Inset in (d): Left: Zoom in of the data where the signal for  $X'X'$  polarization is divided by 100 to demonstrate the lack of detectable *leakage* into cross polarization. Right: Top view of the Fe-As layer for the  $\text{LiFeAs}$  crystal structure and the  $XY-X'Y'$  coordinates.

the  $\text{NaFe}_{1-x}\text{Cu}_x\text{As}$  structure would have the same point-group symmetry as the  $\text{LiFeAs}$  structure. By symmetry,

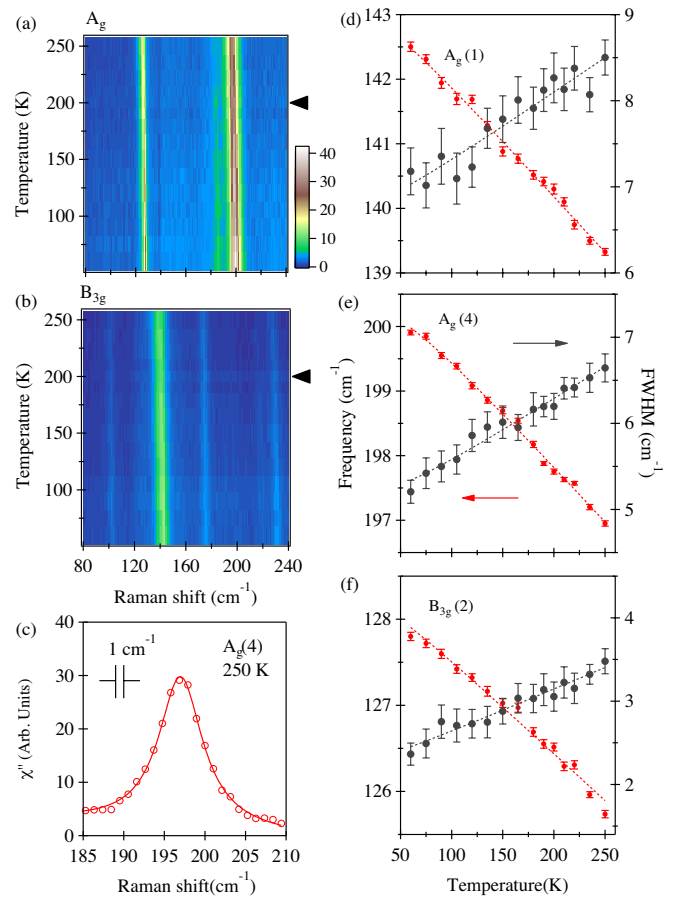


FIG. 3. For  $\text{NaFe}_{0.53}\text{Cu}_{0.47}\text{As}$  crystals, temperature dependence of the Raman response in (a)  $A_g$  and (b)  $B_{3g}$  symmetry channels measured with 1.9 eV laser excitation. The spectral resolution is  $1 \text{ cm}^{-1}$ . Black arrows indicate the magnetic phase transition at 200 K. (c) Lorentz fit to the  $A_g(4)$  phonon at 250 K. Inset: Spectral resolution. (d-f) Temperature dependence of the phonon peak frequency for the  $A_g(1)$ ,  $A_g(4)$ , and  $B_{3g}(2)$  modes. Vertical error bars are one standard deviation error of the Lorentzian fit. Dashed lines show fits of the phonon frequency and line width to Eqs. (1) and (2).

no Raman-active phonons are allowed in the  $XY$  scattering geometry for the  $\text{LiFeAs}$  structure. As we demonstrate in the inset in Fig. 2(d), the *leakage* intensity for the tetragonal  $\text{LiFeAs}$  structure is less than a percent.

Based on the Raman scattering selection rules, we can deduce that the *leakage* intensity is proportional to  $(b-c)^2/4$  (Table I), which is a measure of the anisotropic electronic properties between the  $Y$  and the  $Z$  directions<sup>15</sup>. The observation of the *leakage* is consistent with the suggested formation of a long range stripe order which breaks the crystallographic four-fold symmetry<sup>6</sup>. The count of observed Raman-active phonons for the  $\text{NaFe}_{1-x}\text{Cu}_x\text{As}$  structure also suggests that the size of its primitive cell is four times larger than that for the  $\text{NaFeAs}$  structure (Table I), therefore, the only possible consistent structure is the Fe-Cu stripe order phase, as shown in the inset in Fig. 1.

TABLE III. Fitting parameters for the frequency and linewidth of the  $A_g(1)$ ,  $A_g(4)$ , and  $B_{3g}(2)$  modes. Units are  $\text{cm}^{-1}$ .

Mode	$\omega_0$	$\omega_1$	$2\Gamma_0$	$2\Gamma_1$
$A_g(1)$	$128.72 \pm 0.07$	$0.49 \pm 0.02$	$2.06 \pm 0.06$	$0.23 \pm 0.02$
$A_g(4)$	$201.51 \pm 0.06$	$1.21 \pm 0.02$	$4.67 \pm 0.07$	$0.53 \pm 0.03$
$B_{3g}(2)$	$143.82 \pm 0.07$	$0.87 \pm 0.02$	$6.4 \pm 0.1$	$0.41 \pm 0.04$

In Figs. 3(a) and (b) we show the intensity plot of the Raman response  $\chi''(\omega, T)$  for  $A_g$  (YY + ZZ) and  $B_{3g}$  (YZ + ZY) symmetry channels between 250 and 60 K. All phonons show a symmetric line shape. The number of phonon modes and their line shapes do not change across the antiferromagnetic phase transition at 200 K, suggesting weak magneto-elastic interaction.

We analyze  $A_g(1)$ ,  $A_g(4)$  and  $B_{3g}(2)$  phonons by fitting to Lorentzian function. As an example, Fig. 3(c) shows the  $A_g(4)$  mode at 250 K and its Lorentzian fit. The fitting results are summarized in Figs. 3(d) and (e). Since the magneto-elastic interaction appears to be undetectable within the experimental resolution, we fit the modes temperature dependence by the anharmonic decay model for the entire temperature range (250 to 60 K)<sup>18</sup>:

$$\omega(T) = \omega_0 - \omega_1 \left[ 1 + \frac{2}{e^{\hbar\omega_0/2k_B T} - 1} \right] \quad (1)$$

$$\Gamma(T) = \Gamma_0 + \Gamma_1 \left[ 1 + \frac{2}{e^{\hbar\omega_0/2k_B T} - 1} \right] \quad (2)$$

The fitting results are summarized in Table III.

## IV. CONCLUSION

In summary, we present a polarization-resolved Raman scattering study of  $\text{NaFe}_{0.53}\text{Cu}_{0.47}\text{As}$  single crystals. We observe four  $A_g$  and four  $B_{3g}$  phonon modes at 126, 172, 183, and 197  $\text{cm}^{-1}$  and 101, 139, 173, and 226  $\text{cm}^{-1}$ , respectively. The results are consistent with the *Ibam* space-group symmetry structure where Fe/Cu atoms form a stripe order. No phonon anomaly is observed across the magnetic phase transition from 250 to 60 K, suggesting weak electron-phonon and magneto-elastic interaction.

## ACKNOWLEDGEMENTS

The spectroscopic work at Rutgers was supported by NSF Grant No. DMR-1709161. Sample characterization (W.Z.) was supported in part by the U.S. Department of Energy, Office of Basic Energy Sciences, Division of Materials Sciences and Engineering under Contract No. DE-SC0005463. The crystal growth at Rice was supported by the U.S. Department of Energy, Office of Basic Energy Sciences, under Contract No. DE-SC0012311 and Robert A. Welch Foundation Grant No. C-1839.

\* [wz131@physics.rutgers.edu](mailto:wz131@physics.rutgers.edu)

† Current address: Department of Applied Physics, Northwestern Polytechnical University, Xi'an 710072, China

‡ [girsh@physics.rutgers.edu](mailto:girsh@physics.rutgers.edu)

<sup>1</sup> G. F. Chen, W. Z. Hu, J. L. Luo, and N. L. Wang, *Phys. Rev. Lett.* **102**, 227004 (2009).

<sup>2</sup> J. D. Wright, T. Lancaster, I. Franke, A. J. Steele, J. S. Möller, M. J. Pitcher, A. J. Corkett, D. R. Parker, D. G. Free, F. L. Pratt, P. J. Baker, S. J. Clarke, and S. J. Blundell, *Phys. Rev. B* **85**, 054503 (2012).

<sup>3</sup> A. F. Wang, J. J. Lin, P. Cheng, G. J. Ye, F. Chen, J. Q. Ma, X. F. Lu, B. Lei, X. G. Luo, and X. H. Chen, *Phys. Rev. B* **88**, 094516 (2013).

<sup>4</sup> G. Tan, Y. Song, R. Zhang, L. Lin, Z. Xu, L. Tian, S. Chi, M. K. Graves-Brook, S. Li, and P. Dai, *Phys. Rev. B* **95**, 054501 (2017).

<sup>5</sup> C. Ye, W. Ruan, P. Cai, X. Li, A. Wang, X. Chen, and Y. Wang, *Phys. Rev. X* **5**, 021013 (2015).

<sup>6</sup> Y. Song, Z. Yamani, C. Cao, Y. Li, C. Zhang, J. S. Chen, Q. Huang, H. Wu, J. Tao, Y. Zhu, W. Tian, S. Chi, H. Cao, Y.-B. Huang, M. Dantz, T. Schmitt, R. Yu, A. H. Nevidomskyy, E. Morosan, Q. Si, and P. Dai, *Nat. Commun.* **7**, 13879 (2016).

<sup>7</sup> C. E. Matt, N. Xu, B. Lv, J. Ma, F. Bisti, J. Park, T. Shang, C. Cao, Y. Song, A. H. Nevidomskyy, P. Dai, L. Patthey, N. C. Plumb, M. Radovic, J. Mesot, and M. Shi, *Phys. Rev. Lett.* **117**, 097001 (2016).

<sup>8</sup> A. Charnukha, Z. P. Yin, Y. Song, C. D. Cao, P. Dai, K. Haule, G. Kotliar, and D. N. Basov, *Phys. Rev. B* **96**, 195121 (2017).

<sup>9</sup> M. A. Tanatar, N. Spyrisson, K. Cho, E. C. Blomberg, G. Tan, P. Dai, C. Zhang, and R. Prozorov, *Phys. Rev. B* **85**, 014510 (2012).

<sup>10</sup> X. Wang, Q. Liu, Y. Lv, Z. Deng, K. Zhao, R. Yu, J. Zhu, and C. Jin, *Science China Physics, Mechanics and Astronomy* **53**, 1199 (2010).

<sup>11</sup> E. Kroumova, M. Aroyo, J. Perez-Mato, A. Kirov, C. Capillas, S. Ivantchev, and H. Wondratschek, *Phase Transit.* **76**, 155 (2003).

<sup>12</sup> A. Gozar, *Ph.D. thesis*, University of Illinois at Urbana-Champaign (2004).

<sup>13</sup> In the set-up, see Fig. 2.1 in<sup>12</sup>, Melles Griot Glan-Taylor polarizing prism with a better than  $10^{-5}$  extinction ratio was used to clean the laser excitation beam and a Karl Lambrecht Corporation broad band polarizing cube with an extinction ratio better than 1:500 was used for the analyzer.

- <sup>14</sup> W.-L. Zhang, Z. P. Yin, A. Ignatov, Z. Bukowski, J. Karpinski, A. S. Sefat, H. Ding, P. Richard, and G. Blumberg, [Phys. Rev. B \*\*93\*\*, 205106 \(2016\)](#).
- <sup>15</sup> S.-F. Wu, W.-L. Zhang, L. Li, H.-B. Cao, H.-H. Kung, A. S. Sefat, H. Ding, P. Richard, and G. Blumberg, (2017), [arXiv:1712.01903](#).
- <sup>16</sup> M. Klein, in *Light Scattering in Solids II. Basic Concepts and Instrumentation*, Chap. 2.
- <sup>17</sup> Y. J. Um, J. T. Park, B. H. Min, Y. J. Song, Y. S. Kwon, B. Keimer, and M. Le Tacon, [Phys. Rev. B \*\*85\*\*, 012501 \(2012\)](#).
- <sup>18</sup> J. Menéndez and M. Cardona, [Phys. Rev. B \*\*29\*\*, 2051 \(1984\)](#).